Atmospheric
Chemistry
and Physics
Discussions

1 **Future changes in the stratosphere-to-troposphere ozone mass flux and the contribution**

2 **from climate change and ozone recovery**

3

4 Stefanie Meul[1], Ulrike Langematz[1], Philipp Kröger[1], Sophie Oberländer-Hayn[1], and Patrick

5 Jöckel[2]

6 [1]Freie Universität Berlin, Berlin, Germany

7 [2]Deutsches Zentrum für Luft- und Raumfahrt (DLR) e.V., Institut für Physik der Atmosphäre,

8 Oberpfaffenhofen, Germany

9

10 **Abstract**

11 Model simulations consistently project an increase in the stratosphere-troposphere exchange

12 (STE) of ozone in the future. Both, a strengthened circulation and ozone recovery in the

13 stratosphere contribute to the increased mass flux. In our study, we investigate with a state-of-

14 the-art chemistry-climate model the drivers of future STE change as well as the change in the

15 distribution of stratospheric ozone in the troposphere. Our focus is on the investigation of the

16 changes on the monthly scale. The global mean influx of stratospheric ozone into the

17 troposphere is projected to increase between the years 2000 and 2100 by 53% under the RCP8.5

18 greenhouse gas scenario. We find the largest increase of STE in the NH in June due to

19 increasing greenhouse gas (GHG) concentrations. In the southern hemisphere (SH) the GHG

20 effect is dominating in the winter months, while decreasing levels of ozone depleting substances

21 (ODS) and increasing GHG concentrations contribute nearly equally to the increase in SH

22 summer. A large ODS-related ozone increase in the SH stratosphere leads to a change in the

23 seasonal breathing term which results in a future decrease of the ozone mass flux into the

24 troposphere in the SH in September and October. We find that the GHG effect on the STE

25   change is due to circulation and stratospheric ozone changes, whereas the ODS effect is

26   dominated by the increased ozone abundance in the stratosphere. The resulting distributions of

27   stratospheric ozone in the troposphere for the GHG and ODS changes differ because of the

28   different regions of ozone input (GHG: midlatitudes; ODS: high latitudes) and the larger

29   increase of tropospheric ozone loss rates due to GHG increase. Thus, the model simulations

30   indicate that stratospheric ozone is more efficiently mixed to lower levels if only ODS levels

31   are changed. The increase of the stratospheric ozone column in the troposphere explains more

32   than 80 % of the tropospheric ozone trend in NH spring and in the SH except for the summer

33   months. The importance of the future stratospheric ozone contribution to tropospheric ozone

34   burdens therefore depends on the season.

Atmospheric
Chemistry
and Physics
Discussions

Open Access

1. Introduction

35

36   Ozone (O_3) in the troposphere has two sources: photochemical production involving ozone

37   precursor species such as nitrogen oxides (NO_x), carbon monoxide (CO) and hydrocarbons

38   (e.g., methane (CH_4)) and the transport of ozone from the stratosphere into the troposphere (i.e.

39   stratosphere-troposphere exchange, STE) (IPCC, 2001). Mass can be exchanged between the

40   stratosphere and the troposphere along isentropic surfaces which intersect the tropopause in the

41   lowermost stratosphere (LMS) (Holton et al., 1995) where the chemical lifetime of ozone is

42   larger than the transport timescale. Tropopause folds in the vicinity of the polar and the

43   subtropical jets and cut-off lows are important structures for the effective transport of

44   stratospheric air masses into the troposphere because of their large displacements of the

45   tropopause on isentropic surfaces (Stohl et al., 2003). Mass exchange is also possible by slow

46   cross-isentropic transport, which is driven by diabatic cooling (Stohl et al., 2003) through the

47   large-scale vertical motion of air in the stratospheric meridional residual circulation, the

48   Brewer-Dobson circulation (BDC).

49   Earlier studies have shown that in a changing climate the mass transport from the stratosphere

50   will increase due to a strengthened BDC (e.g., Scaife and Butchart, 2001; Butchart et al.,

51   2010; Oberländer et al., 2013). Akritidis et al. (2016) found coinciding increases in the

52   frequency of tropopause folds in summer over the Eastern Mediterranean and in stratospheric

53   ozone in the lower troposphere between 1979 and 2013. In addition to changes in the ozone

54   transport from the stratosphere into the troposphere, ozone concentrations in the stratosphere

55   are expected to change. Due to declining halogen levels in the stratosphere following the

56   regulation of ozone depleting substances (ODS) by the Montreal Protocol and its

57   amendments, stratospheric ozone is projected to recover during the 21st century (e.g., WMO,

58   2014). In addition, radiative cooling of the stratosphere associated with the rising

59   concentrations of well-mixed greenhouse gases (GHG) (i.e. carbon dioxide (CO_2), nitrous

60   oxide (N_2O) and CH_4) will lead to reduced ozone loss rates and an ozone increase in the

61   stratosphere (e.g., Jonsson et al., 2004). Both, the intensified stratospheric circulation, and the

62   concurrent recovery of stratospheric ozone are expected to lead to an increase in the ozone

63   mass entering the troposphere (e.g., Stevenson et al., 2006; Shindell et al., 2006; Hegglin and

64   Shepherd, 2009; Young et al., 2013; Banerjee et al., 2016). Previous studies with different

65   models and approaches have indicated a dominant role of stratospheric circulation changes for

66   the increased STE (e.g., Sudo et al., 2003; Zeng and Pyle, 2003; Collins et al., 2003). Also in

67   observational data, the connection between stratospheric circulation changes and tropospheric

68   ozone variations was identified (Neu et al., 2014). However for the past, Ordóñez et al. (2007)

69   showed that changes in lowermost stratospheric ozone concentrations have a larger effect on

70   the STE change than variations in cross-tropopause air mass transport. A reduced STE due to

71   stratospheric ozone depletion in the past was found by Shindell et al. (2006) to offset more

72   than half of the tropospheric ozone increase since preindustrial times. The influence of

73   stratospheric ozone recovery on STE in the future was reported by Zeng et al. (2010) who

74   showed that in the Southern Hemisphere (SH) during winter stratospheric ozone increase and

75   climate change have a nearly equal contribution to the increase in surface ozone under the

76   A1B scenario. More recently, the drivers of future STE changes have been analysed by

77   Banerjee et al. (2016) in idealized model simulations. They find that ODS and climate change

78   under the RCP8.5 scenario contribute about equally to the annual global STE increase

79   between 2000 and 2100.

80   Rising GHG concentrations, however, do not only affect the stratospheric circulation and

81   chemistry. In the troposphere, GHG-induced warming increases the water vapour content and

82   thus tropospheric ozone destruction (e.g., Johnson et al., 1999). This results in a decrease of

83　　chemical ozone lifetimes (e.g., Zeng et al., 2010; Banerjee et al., 2016) which means that the

84　　distribution and the burden of stratospheric ozone entering the troposphere are also altered.

85　　In addition to a changing amount of stratospheric ozone in the troposphere, changing future

86　　emissions of ozone precursor species will affect the local ozone production in the troposphere.

87　　Large differences exist in the temporal evolution of the emissions between the Representative

88　　Concentration Pathways (RCP) for the radiative forcing of 6.0 W/m^2 and 8.5 W/m^2

89　　(Meinshausen et al., 2011), especially for CH_4. This will result in a larger ozone production

90　　under the RCP8.5 scenario at the end of the 21st century compared to the RCP6.0 scenario. As

91　　a consequence, the importance of stratospheric ozone in the troposphere in the future will

92　　depend on the net tropospheric chemical ozone production.

93　　Most studies addressing the question of future STE changes and their role for tropospheric

94　　ozone trends focus on the annual and global integrated fluxes. Hegglin and Shepherd (2009)

95　　showed also the annual cycle of the ozone mass flux derived from a boxmodel approach

96　　introduced by Appenzeller et al. (1996). In their model simulation, the maximum ozone flux

97　　occurs in spring in the SH and Northern Hemisphere (NH) for the 1960 to 1970 mean. In the

98　　future (2090-2100), the peak is shifted towards late spring/early summer in the NH and towards

99　　winter in the SH. As Roelofs and Lelieveld (1997) reported, the seasonal timing of the input of

100　stratospheric ozone into the troposphere is relevant for potential mixing of stratospheric ozone

101　towards the surface, since in summer the ozone loss rate is larger than in winter. This means

102　that the future distribution of stratospheric ozone in the troposphere depends not only on the

103　overall increase on ozone mass flux, but also on the seasonality of the input.

104　The aim of our study is therefore, to quantify the future changes of STE in idealized simulations

105　with a chemistry-climate model (CCM) under the most extreme RCP8.5 scenario for the annual

106　and monthly means. We identify the changes in the seasonal cycle of STE due to the projected

107　increase in GHGs and decline in ODS, i.e. the associated stratospheric ozone recovery.

108 Furthermore, we analyse the resulting changes in the distribution of stratospheric ozone in the

109 troposphere, using comprehensive stratospheric and tropospheric chemistry and therefore

110 considering the full range of changes in chemical loss and production caused by GHG or ODS

111 changes. The additional analysis with a transient run under the RCP6.0 scenario allows us on

112 the one hand to study the past changes between 1960 and 1999 and on the other hand to compare

113 two different scenarios and their effect on stratospheric ozone trends in the troposphere.

114 In this study we want to address the following research questions:

115 (1) How will the stratosphere-to-troposphere ozone mass flux change in the future?

116 (2) What are the major drivers of the future changes in the stratosphere-to-troposphere ozone

117 mass flux?

118 (3) Will the seasonality of the STE change in future?

119 (4) How will the GHG emission scenarios affect the ozone mass flux into the troposphere?

120 (5) How is the ratio of stratospheric ozone in the troposphere changed in the future?

121 The study is structured as followed: First the model and the experimental set-up used for the

122 simulations are described as well as the methodology for calculating the ozone mass flux from

123 the stratosphere to the troposphere (Section 2). In Section 3 we show the climatological mean

124 state of the year 2000 simulation for a basic evaluation. Results of mass flux changes and

125 changes in the distribution of stratospheric ozone in the troposphere are shown in Section 4

126 followed by the attribution analysis in Section 5. The results are summarized in Section 6.

127

128 **2. Model experiments and methods**

129 **2.1 Model experiments**

130 In this study we applied the EMAC (ECHAM/MESSy Atmospheric Chemistry) CCM version

131 described by Jöckel et al. (2016) in the T42L47MA configuration, i.e. with 47 model layers and

132   a horizontal resolution of 2.8°x2.8°. EMAC is a numerical chemistry and climate simulation

133   system that includes submodels describing tropospheric and middle atmosphere processes and

134   their interaction with oceans, land and human influences (Jöckel et al., 2016). It uses the second

135   version of the Modular Earth Submodel System (MESSy2) to link multi-institutional computer

136   codes. The core atmospheric model is the 5th-generation European Centre Hamburg general

137   circulation model (ECHAM5) (Roeckner et al., 2006). The atmospheric chemistry is calculated

138   using the submodule MECCA (Module Efficiently Calculating the Chemistry of the

139   Atmosphere; revised version by Sander et al., 2011a). The gas-phase rate coefficients follow

140   the latest recommendations of JPL (Sander et al., 2011b). For heterogeneous reactions in the

141   stratosphere the rate coefficients are calculated with the submodel MSBM (Multi-phase

142   Stratospheric Box Model) which also returns the parameters (e.g., number densities, surface

143   areas) of the sulfuric acid aerosols and the polar stratospheric cloud (PSC) particles.

144   To quantify the impact of increasing GHG concentrations and of declining stratospheric

145   halogen levels on the net ozone mass flux from the stratosphere into the troposphere, we

146   performed four experiments in timeslice mode, i.e. with non-varying boundary conditions from

147   year to year, but including a seasonal cycle. In addition to reference simulations for the years

148   2000 and 2100, one sensitivity simulation for GHG increase only and one for ODS decrease

149   only have been set up. Each timeslice simulation has been integrated over 40 years following 5

150   years of spin-up time. Future surface concentrations of the well-mixed GHGs (CO_2, N_2O, CH_4)

151   are prescribed according to the extreme RCP8.5 scenario (Meinshausen et al., 2011) in order to

152   reveal the upper boundary of the anticipated future changes. The estimated decline of ODS as

153   a consequence of the successful regulation of halogen containing species in the Montreal

154   Protocol and its amendments is given by the boundary conditions following the A1 scenario in

155   WMO (2011). Note that due to an unintended neglect of minor chlorine source gases CFC-113,

156   CFC-144, CFC-155 as well as HCFC-22, HCFC-141b and HCFC-142b, stratospheric chlorine

157   levels in the year 2000 are underestimated by about 10%. The quasi-biennial oscillation (QBO)

158   of tropical winds in the stratosphere is nudged to observations following Giorgetta and

159   Bengtsson (1999). Solar variability like the 11-year solar cycle is not included, instead solar

160   mean conditions of solar cycle number 22 are prescribed. The sea surface temperature (SST)

161   and sea ice concentration (SIC) fields are prescribed as 10-year averages around the respective

162   years using the output from a transient simulation with the coupled atmosphere ocean model

163   MPI-ESM (Max-Planck-Institute Earth System Model; Giorgetta et al., 2013; Schmidt et al.,

164   2013) for the RCP8.5 scenario. Using multi-year averages reduces the inter-annual variability

165   of the SSTs, but ensures quasi neutral conditions of the El Niño Southern Oscillation (ENSO).

166   An overview of the boundary conditions in the four simulations is given in Table 1.

167   To show the temporal evolution of the changes and to compare the effects for different GHG

168   scenarios we also analyse the model output from the transient simulation RC2-base-05 of the

169   Earth System Chemistry integrated Modelling (ESCiMo) project (Jöckel et al., 2016) which has

170   been integrated according to the RCP6.0 scenario from 1960 to 2100 following a 10-year spin-

171   up. The SST and SIC fields for the RCP6.0 scenario are prescribed from the Hadley Centre

172   Global Environment Model version 2 - Earth System (HadGEM2-ES) Model (Collins et al.,

173   2011; Martin et al., 2011). The boundary conditions for this simulation are given in Table 1.

174   More detailed information of this simulation can be found in Jöckel et al. (2016). It has to be

175   noted, that the stratospheric ozone loss in the past is underestimated in this simulation, which

176   affects the trends in ozone mass flux.

177   **2.2 Methods**

178   To quantify the net ozone mass flux from the stratosphere into the troposphere we apply the

179   boxmodel approach described by Appenzeller et al. (1996). They described the hemispheric net

180   mass transport in a simple model which consists of three regions (i.e. boxes), the troposphere,

Atmospheric
Chemistry
and Physics
Discussions

181   the 'lowermost stratosphere' (LMS) and the 'overworld'. The LMS is the region where isentropic

182   surfaces intersect the tropopause. Thus mass can be exchanged between the stratosphere and

183   the troposphere along such isentropic surfaces. Above the LMS, often referred to as the

184   overworld according to Holton et al. (1995), the isentropic surfaces lie entirely in the

185   stratosphere and mass exchange is only possible by cross-isentropic transport, which is carried

186   out by the large-scale meridional circulation in the stratosphere (BDC). Due to mass continuity,

187   a mass flux from the overworld into the LMS (F_{in}) must be balanced by a mass flux out of the

188   LMS (F_{out}) and/or mass change (dM/dt) in the LMS:

189     $F_{in} = F_{out} + dM/dt$ (1).

190   In our study we use the 91 hPa surface (nearest pressure level of the model output to 100 hPa)

191   as upper boundary for the LMS boxmodel and the model tropopause (a combination of the

192   thermal tropopause in the tropics and the dynamical tropopause in the extratropics) as lower

193   boundary, analogously to Hegglin and Shepherd (2009). Thus, M in Equation 1 is the total

194   ozone mass between these boundaries, and dM/dt is the monthly change of M. F_{in} is calculated

195   for each hemisphere as the area-weighted integral of the product of the monthly zonal mean

196   ozone concentration and the negative of the monthly mean residual vertical velocity ($-\overline{w}^*$) at 91

197   hPa at each gridpoint. Since, by definition, the vertical velocity is positive for upward and

198   negative for downward motion, $\overline{w}^*$ is multiplied by the factor -1 in order to get positive values

199   for the downward ozone mass flux into the troposphere. Finally, F_{out} is calculated as residual.

200   It has to be noted that with this methodology it is not possible to study the transport pathways.

201   The use of the 91 hPa surface as upper boundary instead of 100 hPa leads to slightly lower

202   values of the resulting ozone mass flux (< 2 % in the REF2000 simulation, estimation based on

203   linear interpolation between the two model pressure surfaces surrounding 100 hPa).

204   To distinguish ozone with stratospheric origin and ozone produced in the troposphere we use a

Atmospheric
Chemistry
and Physics
Discussions

205   diagnostic tracer O3s (Roelofs and Lelieveld, 1997; Collins et al., 2003; Jöckel et al., 2016).

206   This tracer is reset in each model time step (by nudging with a relaxation time equaling the

207   model time step length) to the interactive ozone above the model tropopause. In the troposphere,

208   the chemical production of O3s is omitted while the sinks of O3s, i.e. chemical loss and dry

209   deposition, are considered in the same way as for O3. The loss of O3s (LO3s) plus the dry

210   deposition have been used as a qualitative measure of STE in earlier studies (e.g., Roelofs and

211   Lelieveld, 1997; Jöckel et al., 2006). However, in our study this different method of STE

212   estimation was not applied since the output of dry deposition for the O3s tracer was not

213   available. Also, LO3s is not only affected by changes in ozone flux but also by changes in

214   tropospheric ozone chemistry due to the prescribed forcings, potentially leading to differences

215   in the derived STE.

216

217   **3.   Equilibrium state of the year 2000 (REF2000)**

218   Before we estimate the future change in ozone mass flux into the troposphere, the present-day

219   equilibrium state is analysed to ensure that the important mixing processes and tracer

220   distributions are represented realistically in the EMAC simulations. An effective method to

221   investigate STE and mixing processes in the LMS are tracer-tracer correlations.

222   **3.1 Tracer-tracer correlations from scatter plots**

223   Fischer et al. (2000) introduced the O_3-CO correlations for aircraft in situ measurements to

224   analyse the chemical transition between the stratosphere and troposphere and the mixing

225   processes in the UTLS. Due to the sharp gradients with high CO (low O_3) values in the upper

226   troposphere and low CO (high O_3) values in the lower stratosphere, the O_3-CO scatter plot has

227   a characteristic L-shape in the UTLS (e.g., Fischer et al., 2000; Tian et al., 2010; Barré et al.,

Atmospheric
Chemistry
and Physics
Discussions
Open Access

EGU

228 2013). Pan et al. (2007) distinguish the stratospheric branch and the tropospheric branch with a

229 quasi linear relation between O_3 and CO and a transition region in between characterized by

230 non-linear behavior. Figure 1 (top) shows the O_3-CO scatter plot for the REF2000 simulation

231 in the northern mid-latitudes. Compared to the results shown by Fischer et al. (2000) for

232 measurements and Barré et al. (2013) for measurements and model data, we find that the L-

233 shape of the correlation is captured reasonably well by the EMAC timeslice simulation.

234 The shape of the O_3-N_2O scatter plot (Figure 1, bottom) with a full stratosphere coverage results

235 from the negative vertical gradient in N_2O and the O_3 maximum in the stratosphere: The

236 correlation is negative below the ozone maximum and positive above. The fan-shaped structure

237 is due to the horizontal gradient with higher O_3 and N_2O values in the tropics than in the extra-

238 tropics. The model result is in qualitative agreement with O_3-N_2O scatter plots for ACE

239 measurements shown by Hegglin and Shepherd (2007).

240 This comparison indicates that the dynamical and chemical processes in the transition region

241 between the troposphere and stratosphere are realistic in the EMAC timeslice simulations and

242 allows us to assess the future changes.

243 **3.2 Ozone mass flux**

244 The annual cycle of the ozone mass flux into the troposphere (F_{out}, calculated according Eqation

245 1) for the year 2000 reference simulation is shown in Figure 2a integrated globally and over the

246 NH and SH respectively. The ozone mass flux into the NH is larger than into the SH and has

247 its peak in early summer, whereas in the SH the maximum ozone mass flux is found in spring.

248 The annual cycle in the EMAC REF2000 simulation is comparable to the results of Hegglin

249 and Shepherd (2009) for the period 1960 to 1970, but with a less pronounced peak in the NH

250 spring in EMAC.

251   Integrated over all months, the ozone mass flux reaches 390 ± 17 Tg/year in the NH, 322 ± 15

252   Tg/year in the SH and 712 ± 24 Tg/year globally. The global ozone mass flux hits the upper

253   boundary of the ozone mass flux derived from tropospheric models for the year 2000 ($552 \pm$

254   168 Tg/year; Stevenson et al., 2006) and is larger than the ozone mass flux reported by Hegglin

255   and Shepherd (2009) (655 ± 5 Tg/year), which was derived by averaging the 1995 to 2005

256   period of a transient simulation with a middle atmosphere resolving CCM. However, the ozone

257   mass flux in the REF2000 simulation lies in the range of 340 – 930 Tg/year given by Collins et

258   al. (2000) for a range of models and agrees well with the ozone mass flux of 770 ± 400 Tg/year

259   given in IPCC (2001). Compared to estimates derived from observations (500 ± 140 Tg/year;

260   Olsen et al., 2002), the ozone mass flux in the EMAC timeslice simulation is slightly

261   overestimated.

262   To better understand the changes in the calculated ozone mass flux ($F_{out} = F_{in} - dM/dt$), we

263   analyse the climatological annual cycle of the two ozone mass flux components, F_{in} at 91 hPa

264   (Figure 2b) and $-dM/dt$ (Figure 2c). The ozone mass flux across the 91 hPa pressure level is

265   controlled by the seasonality of the BDC with the maximum (ozone) mass transport in the

266   winter hemisphere and a hemispherically asymmetric strength. The ozone distribution in the

267   stratosphere (see also Figure 3a) with low columns in the tropics and high columns in the middle

268   and high latitudes also reflects the structure of the stratospheric meridional circulation.

269   The seasonal breathing of the LMS leads to a shift of the maximum ozone mass flux from winter

270   to spring (Hegglin and Shepherd, 2009). The amplitude of the seasonal cycle in $-dM/dt$ is

271   slightly larger in the NH than in the SH which dampens the amplitude of the ozone mass flux

272   in the NH.

273   The timing of the maximum ozone mass flux into the troposphere is relevant for the resulting

274   downward mixing since the chemical lifetime of tropospheric ozone in the mid- and high

275   latitudes has a pronounced seasonal cycle with short lifetimes in the summer and relatively long

276   lifetimes in winter and spring. This means that ozone can be mixed more efficiently with

277   tropospheric air masses in winter and spring (Roelofs and Lelieveld, 1997) although the ozone

278   influx from the stratosphere is smaller than in summer.

279   In the next section we analyse the abundance of stratospheric ozone in the troposphere for June

280   (Figure 3), when the ozone mass flux is maximal in the NH and minimal in SH (Figure 2a).

3.3 Stratospheric ozone in the troposphere

282   In the troposphere, the columns of ozone originating from the stratosphere (Figure 3b) reach a

283   maximum of 30 DU around 30° in both hemispheres and a minimum in the tropics (3-6 DU

284   over Indonesia) and the southern high latitudes. The low values in the tropics presumably result

285   from very short ozone lifetimes near the surface as the high insolation and high water vapour

286   concentrations in the intertropical convergence zone (ITCZ) form a strong sink for tropospheric

287   ozone (Roelofs and Lelieveld, 1997). In addition, the downward transport of stratospheric

288   ozone in the tropics is very small due to the upward branch of the BDC in this region. The high

289   O3s columns in the subtropics result from high abundances of stratospheric ozone in the upper

290   troposphere, especially in the NH subtropics, which is evident in Figure 3c. Here, ozone

291   entering the troposphere through tropopause folds is efficiently transported to lower altitudes

292   in the downward branch of the Hadley cell (Roelofs and Lelieveld, 1997) resulting in relatively

293   high O3s levels in the middle troposphere around 30°N. The O3s mixing ratios decrease with

294   lower altitude and reach their minimum near the surface, with the smallest values in the tropics

295   and the NH, since ozone loss is largest in summer (Figure 3d). However, ozone originating

296   from the stratosphere is also found down to the lower troposphere in the extra-tropics. This may

297   be caused by events when stratospheric air penetrates deep into the troposphere and affects also

298   lower levels (e.g., Škerlak et al., 2014).

299 The contribution of O3s to ozone is in the range between 20 % in the tropics and the NH lower

300 troposphere and up to 40 % in the middle troposphere (500 hPa) in the NH. In the SH, the

301 relative contribution of O3s to O_3 is larger (50-60 % near the surface and more than 60 % at

302 500 hPa at high latitudes). This is caused by low chemical loss of O3s in winter (Figure 3d) in

303 combination with small chemical production of tropospheric ozone in this season. In SH

304 summer this pattern is reversed (not shown), however, with a slightly larger contribution of O3s

305 near the SH surface (20-30 %) compared to NH summer. This is possibly related to the lower

306 local photochemical ozone production in the SH due to reduced emissions and abundances of

307 tropospheric ozone precursor species.

308 In summary, we have found realistic tracer distributions in the tropopause region of the EMAC

309 reference simulation for the year 2000. The ozone mass flux appears to be overestimated

310 compared to observations and other model studies, while lying within the range estimated in

311 IPCC (2001). Given the large uncertainties for estimates from observational data and the range

312 of different model types, the ozone mass flux in EMAC can be regarded as reasonable. The

313 results indicate that the important processes determining the STE are sufficiently well

314 reproduced by EMAC, which allows us to study in the next section the past and future changes

315 of the ozone mass flux as well as the contributions from GHG and ODS changes.

316

317 **4. Past and future changes in ozone mass flux into the troposphere**

318 Changes in the input of stratospheric ozone into the troposphere can be caused by changes in

319 the dynamical processes and/or by the amount of ozone that is available for transport in the

320 stratosphere. Thus, not only GHG concentrations may have an impact on the stratosphere-to-

321 troposphere transport but also the development of ODS. The temporal evolution between 1960

322 and 2099 of the integrated ozone mass flux for the RCP6.0 simulation, which includes both, the

Atmospheric
Chemistry
and Physics
Discussions

323   observed, and projected ODS and GHG changes, is shown in Figure 4. In the past (1960-1999),

324   the integrated ozone mass flux exhibits a negative trend in both hemispheres with a larger

325   change of -1.4 %/decade in the SH which is in qualitative agreement but smaller than the trend

326   (-2.3 %/decade) found by Hegglin and Shepherd (2009) between 1965 and 2000. Zeng et al.

327   (2010) showed that this negative trend is associated with the ODS-induced ozone loss in the

328   stratosphere which is most prominent in the southern polar region in spring. Between 2000 and

329   2099 the ozone mass flux is projected to increase globally by 4.2 %/decade. Again, the change

330   in the SH (4.9 %/decade) is slightly larger than in the NH (3.7 %/decade). This increase may

331   be the consequence of different forcings: (1) the regulations of ODS emissions lead to a decline

332   of chlorine in the stratosphere and increasing stratospheric ozone levels; (2) the increasing GHG

333   concentrations alter the temperature structure of the atmosphere and intensify the large-scale

334   mass transport in the stratosphere, and (3) the radiative cooling of the stratosphere due to

335   increasing GHG concentrations slows chemical loss reactions, which increases the ozone

336   amount in the stratosphere. To understand the impact of ODS and GHG changes on the ozone

337   mass flux in more detail, we further analyse the sensitivity simulations following the RCP8.5

338   scenario. For comparison the reference timeslice simulations for the years 2000 and 2100 are

339   included in Figure 4. The 1995-2004 average in the RCP6.0 simulation gives an ozone mass

340   flux of 688 ± 24 Tg/year which is slightly lower than in the timeslice simulation for 2000, but

341   within the range of two standard deviations of the REF2000 simulation. This difference might

342   be due to the reduced variability in the timeslice simulation compared to the transient one (see

343   Section 2), and/or due to the different SST/SIC fields used in the simulations. However, the

344   results of the model simulations are in relatively good agreement.

345   In the future, the ozone mass flux is clearly larger in the timeslice simulations than in the

346   transient simulation due to the more extreme GHG emission scenario (RCP8.5 compared to

347   RCP6.0). The integrated ozone mass flux reaches 598 ± 29 Tg/year in the NH, 490 ± 23 Tg/year

348 in the SH and 1088 ± 43 Tg/year for the global sum. This corresponds to a relative increase of

349 5.3, 5.2 and 5.3 %/decade, respectively (see also Table 2). Thus, in contrast to the transient

350 RCP6.0 simulation, the future ozone mass flux change in the RCP8.5 timeslice simulations is

351 similar in the NH and in the SH.

352

353 **5. Attribution of future changes in ozone mass flux to climate change**

354 Figure 5 shows the monthly changes of the ozone mass flux for the sensitivity simulations, i.e.

355 for the total change between 2000 and 2100 due to all forcings and the contributions from GHG

356 and ODS changes. It has to be noted that the changes due to GHGs and ODS do not necessarily

357 sum up to the total change because of non-linear interactions and the missing change in

358 tropospheric ozone precursor species in the ODS-only and GHG-only simulations (see Table

359 1).

360 The change in ozone mass flux between 2000 and 2100 due to all forcings (top row) is positive

361 throughout the year with maximal increases in the summer months of the respective

362 hemispheres by up to 32 Tg/month (75 %) in the NH and 19 Tg/month (68 %) in the SH. The

363 GHG (middle row) and ODS (bottom row) induced changes clearly indicate the dominant role

364 of rising GHG concentrations for the future ozone mass flux change in the NH, explaining 80

365 to 95 % of the total change. The GHG-related ozone mass flux increase in the NH is maximal

366 in June and July, slightly shifting the peak in the annual cycle to summer which is consistent

367 with the findings by Hegglin and Shepherd (2009) for the total change between the 1960-1970

368 and 2090-2100 means. The ODS decrease, however, leads only to small positive and (not

369 significant) negative changes in the NH.

370   In the SH, the GHG-induced increase dominates the ozone mass flux change in winter and

371   spring, but in summer the ODS-related increase of the ozone mass flux contributes up to 50 %

372   to the total change in the SH. A significant reduction of ozone mass flux is found from August

373   to October in the SH due to the ODS change. This causes a shift of the SH maximum ozone

374   flux from October to January and is in contrast to the results by Hegglin and Shepherd (2009)

375   who found the maximum SH ozone mass flux in the future (2090-2100) to occur in August.

376   Overall we find that the GHG-induced changes will determine the positive trend of the ozone

377   mass flux in the NH, while in the SH both ODS and GHG changes affect the trend and the

378   seasonality of the future ozone mass flux into the troposphere.

379   To identify the processes behind the ODS- and GHG-induced changes, we analyse the changes

380   of the two ozone mass flux components, i.e. F_{in} and the seasonal breathing term. We find that

381   F_{in} will increase in the future throughout the year in both hemispheres and for both external

382   forcings. Figure 6 shows in the top row the latitudinal distribution of the product of ozone

383   concentration and $-\overline{w}^*$ at 91hPa, which equals F_{in}, when integrated over all latitudes. The two

384   components of F_{in}, $-\overline{w}^*$ and the ozone concentration, are shown separately in the middle and

385   bottom rows of Figure 6, respectively. The increase of F_{in} (or O_3 x $-\overline{w}^*$) due to the GHG effect

386   (Fig. 6d) is caused by an increase in the downwelling (i.e. $-\overline{w}^*$, positive for downwelling, Fig.

387   6e) of the BDC in the winter season with climate change (e.g., Sudo et al., 2003; Butchart et

388   al., 2010; Oberländer et al., 2013) in combination with an ozone increase resulting from

389   stratospheric cooling and enhanced meridional transport (Figure 6f). In contrast, with ODS

390   decrease no significant changes in the downwelling occur (Figure 6h). The small increase in F_{in}

391   (Figure 6g) is therefore attributed to stratospheric ozone recovery from ODS, in particular in

392   Antarctic spring (Figure 6i). Figure 6 also indicates that the maximum change in ozone mass

393   flux into the troposphere occurs at midlatitudes for the GHG increase and at high latitudes for

Atmospheric
Chemistry
and Physics
Discussions

394   the ODS reduction. This may have an influence on the mixing and distribution of stratospheric

395   ozone in the troposphere (see below).

396   Thus, given the positive changes in F_{in}, the significant negative change in the ozone mass flux

397   identified in September and October for the ODS decrease, must be attributed to changes in –

398   dM/dt (i.e. the monthly change in the ozone mass contained in the LMS, also referred to as

399   seasonal breathing). While the total mass in the LMS is decreasing with rising GHG

400   concentrations in the sensitivity simulations (possibly due to the tropopause lifting effect of

401   rising GHGs), it slightly increases with ODS change only (not shown). The mass of ozone (M),

402   however, is increasing globally due to both, GHGs and ODS. Thus, for the GHG effect, the

403   future increase of ozone in the LMS outweighs the reduction in total LMS mass. If this future

404   increase of M in the LMS is monthly varying, a future change (positive or negative) in –dM/dt

405   will result. Exactly this is happening in SH spring, when the ozone mass increase is steadily

406   amplified between August and November due to the decline of ODS. This results in the shift of

407   the seasonality of the ozone mass flux and therefore to negative changes in SH spring.

408   As mentioned above, the timing of the strongest input of stratospheric ozone into the

409   troposphere is relevant in that the efficiency of mixing down to lower altitudes or to the surface

410   depends on the chemical lifetime of ozone which varies with season. A shift of the spring

411   maximum in the SH to summer (January) for instance may result in different mean abundances

412   of O3s in the troposphere. Furthermore, the chemical loss of ozone will increase in a warmer

413   troposphere, affecting the lifetime of ozone and thus the distribution of stratospheric ozone in

414   the troposphere.

415   The future changes in the distribution of O3s mixing ratios are shown in Figure 7 for June. O3s

416   is projected to increase throughout the extra-tropical troposphere. The largest changes will

417   occur in the subtropics in the upper and middle troposphere, the regions where cross-tropopause

Atmospheric
Chemistry
and Physics
Discussions

418   transport along isentropic surfaces is possible and ozone is efficiently transported into the

419   troposphere through tropopause folds. This pattern is caused by the rising GHG concentrations

420   (Figure 7b). Near the surface however, the O3s mixing ratios will decrease with GHG change

421   at summer NH mid-latitudes, either induced by an increased chemical O3s loss or dry

422   deposition. The total positive change near the surface results from the O3s increase due to ODS

423   change (Figure 7c). In the SH, the abundance of stratospheric ozone increases throughout the

424   troposphere down to the surface. More O3s seems to be transported further down than in the

425   NH, which may be related to the longer chemical lifetime of ozone in winter. This is also

426   obvious from the ODS-induced changes, albeit with very small signals.

427   The annual mean column-integrated values of O3s and ozone in the troposphere and their

428   respective changes are listed in Table 3. The O3s column increases globally by 42 % between

429   the years 2000 and 2100, with a larger change occurring in the SH than in the NH. Consistent

430   with the results above, the main contribution is from the GHG changes, whereas the ODS

431   changes have the largest effect on the SH (+ 6 %). These changes may result from the

432   combination of an increased/monthly shifted ozone mass flux into the troposphere, increased

433   chemical loss of O3s and changes in dry deposition of O3s. The increase in the total burden of

434   tropospheric ozone between 2000 and 2100 (derived from Table 3) indicates that the main

435   contribution to the change is from O3s (19 %), whereas ozone produced in the troposphere

436   (calculated as residual) causes an increase of 12 % summing up to a total increase of 31 % of

437   tropospheric ozone. The larger increase in the chemical loss of O3s compared to the increase in

438   the ozone mass flux indicates changing chemical conditions in the troposphere due to climate

439   change. This means that the larger amount of stratospheric ozone entering the troposphere does

440   not accumulate to the equivalent larger abundance of O3s in the troposphere.

Atmospheric
Chemistry
and Physics
Discussions

441 Next we investigate, to what extent the future change in O3s (Figure 8, middle row) contributes

442 to the ozone change (Figure 8, top row) in the troposphere. The relative contribution is shown

443 in Figure 8 (bottom row) as annual cycle of the tropospheric columns for (c) the change between

444 2000 and 2100 due to all forcings, (f) the respective change due to GHGs, and (i) the respective

445 change due to ODS. We find that at SH middle and high latitudes more than 80 % of the increase

446 in tropospheric ozone column is caused by ozone originating from the stratosphere from April

447 through October. A similar strong contribution to the overall change of more than 80 % occurs

448 in the NH extratropics, however confined to the spring season (March, April and May). For the

449 rest of the year, ozone originating from the stratosphere causes more than 50 % of the total

450 change in both hemispheres. In contrast, in the tropics only 20 to 50 % of the ozone change are

451 attributable to changes in ozone from the stratosphere throughout the year.

452 In addition, our simulations illustrate that the future enhancement of stratospheric ozone import

453 into the troposphere and the resulting tropospheric ozone change will be dominated by the GHG

454 effect. If only the concentrations of ODS would decline between the years 2000 and 2100, a

455 minor increase in tropospheric ozone burden in the (mainly SH) extratropics would form

456 (Figure 8g), which is almost completely attributable to increased stratospheric ozone entering

457 into the troposphere (Figures 8h, 8i). However, only in the simulation with increased GHG

458 concentrations, the patterns and the amount of tropospheric ozone increase (Figure 8d) and the

459 contribution of stratospheric ozone to this increase (Figure 8e), as shown in the simulation with

460 all forcings (Figures 8a, 8b), are well reproduced. Up to 80 % of the tropospheric ozone trends

461 in SH winter and 70 % in NH spring can be explained by increased abundances of stratospheric

462 ozone due to the GHG effect (Figure 8f). These numbers also indicate the strong increase of

463 tropospheric photochemical ozone production in the future due to the doubling of methane

464 emissions under the RCP8.5 scenario (e.g., Young et al., 2013; Meul et al., 2016). In NH

465 summer, about 50 % of the change are due to stratospheric ozone, while in the tropics and the

466   SH summer months, the contribution is less than 40 %. This reflects the effect of the

467   substantially increased ozone loss rates resulting from the more tropical/subtropical downward

468   transport of stratospheric ozone with enhanced GHG concentrations. The chemical ozone loss

469   rate in the troposphere in the ODS simulation is less influenced and nearly unchanged in the

470   tropics. In summary, Figure 8 shows that the input of stratospheric ozone is the dominant driver

471   of ozone changes in the troposphere, if only ODS levels are reduced. For the GHG increase we

472   find that other processes, such as tropospheric chemistry, modulate the tropospheric ozone

473   abundance in addition to the increased influx of stratospheric ozone.

474   Finally, we compare the tropospheric O3s columns derived from the timeslice simulations

475   under the RCP8.5 scenario with the transient simulation using the RCP6.0 scenario. Figure 9a

476   shows the evolution of annual mean tropospheric ozone (solid) and O3s (dashed) columns for

477   the NH and the SH. Tropospheric ozone increases in the RCP6.0 simulation from 1960 to the

478   middle of the 21st century and slightly declines afterwards in the NH, while it stays nearly

479   constant in the SH. There is very good agreement of the tropospheric ozone column between

480   the transient and timeslice simulations for the year 2000, when both simulations use observed

481   GHG concentrations. Regarding the temporal evolution of O3s, we find a positive trend in both

482   hemispheres and only a slight decrease in the NH at the end of the 21st century. In the past, an

483   effect of the ODS driven stratospheric ozone loss is overlaid by the GHG related increase in

484   both hemispheres. However, a slightly smaller rise of O3s in the SH might be an indication.

485   The RCP8.5 scenario (circles) leads to higher values of tropospheric ozone in 2100 which is

486   related to two effects: a larger import of stratospheric ozone and a larger chemical ozone

487   production in the troposphere due to strongly enhanced methane concentrations in the second

488   half of the 21st century in the RCP8.5 scenario (see Meinshausen et al., 2011).

489 The ratio between O3s and tropospheric ozone (Figure 9b) gives an indication if the role of

490 stratospheric ozone in the troposphere will change in the future. In the past period of the

491 transient simulation (i.e. RCP6.0 scenario), the relative contribution of O3s decreases from 48

492 % (1960s) to 44 % (1990s) in the NH and from 52 % to 48 % in the SH. This is caused by an

493 increase of ozone produced in the troposphere, which is stronger than the increase of O3s

494 (Figure 9a). In the future, however, the relative importance of ozone from the stratosphere

495 increases, reaching 49 % in the NH and 55 % in the SH around the year 2100. Thus, in the

496 RCP6.0 scenario (more than) half of the ozone in the troposphere will originate from the

497 stratosphere in the (SH) NH at the end of the 21st century.

498 The comparison with the timeslice simulation (RCP8.5 GHG scenario) shows that the

499 abundance of O3s in the troposphere is lower in the year 2000 than in the transient simulation.

500 This is probably caused by the different data sets used for the SST/SIC fields in the timeslice

501 and transient simulation (see Table 1) leading to different tropopause heights and therefore to

502 different tropospheric columns. However, the larger contribution of O3s to ozone in the SH (48

503 %) compared to the NH (43 %) is confirmed. In 2100, tropospheric ozone columns in the NH

504 (SH) will consist to 46 % (52 %) of ozone originating from the stratosphere. Thus, the increase

505 in the contribution of O3s in the future is slightly smaller in the RCP8.5 scenario than in the

506 RCP6.0 scenario, despite the larger increase in ozone mass flux shown in Figure 2. Here, the

507 different evolution of tropospheric ozone production in the two GHG scenarios plays a crucial

508 role.

509

510 **6. Summary**

511 In this study we have analysed the future changes in stratosphere-to-troposphere transport of

512 ozone in timeslice and transient simulations with the CCM EMAC to address the questions

Atmospheric
Chemistry
and Physics
Discussions

Open Access

513   brought up in the introduction: (1) How will the stratosphere-to-troposphere ozone mass flux

514   change in the future? (2) What are the major drivers of the future changes in stratosphere-to-

515   troposphere ozone mass flux? (3) Will the seasonality of the STE change in future? (4) How

516   will the GHG emission scenarios affect the ozone mass flux into the troposphere? (5) How is

517   the ratio of stratospheric ozone in the troposphere changed in the future?

518   In agreement with other studies (e.g., Sudo et al., 2003; Collins et al., 2003; Hegglin and

519   Shepherd, 2009; Banerjee et al., 2016), we find that the influx of stratospheric ozone into the

520   troposphere will increase in the future. Between 2000 and 2100 the EMAC timeslice

521   simulations project an increase of the annual global mean ozone mass flux by 53 % under the

522   RCP8.5 scenario. Increasing GHG concentrations were identified as the main driver of the

523   rising ozone mass flux into the troposphere by strengthening the BDC and reducing chemical

524   ozone loss in a colder stratosphere. The annual global ozone mass flux is increased by 46 %

525   due to rising GHG concentrations compared to an increase of 7 % due to the ODS decline and

526   the associated ozone recovery. The GHG effect leads to a larger intensification of STE in the

527   NH (51 %) than in the SH (40 %), whereas the ODS effect is most prominent in the SH (9 %)

528   compared to 4 % in the NH.

529   Regarding the seasonal changes of the ozone mass flux, we showed the dominant role of GHG

530   changes for the NH whereas in the SH, both ODS and GHG changes affect the seasonality of

531   the ozone mass flux increase: the GHG increase is the main driver of the increase in winter and

532   spring, but in summer also ODS-induced changes contribute to the ozone mass flux increase.

533   Furthermore, the ODS decrease and the concomitant ozone increase in the lower stratosphere

534   during SH spring cause a large change in the seasonal breathing term in the SH from August to

535   October, which results in a shift of the maximum ozone flux to late spring/early summer. The

536   GHG effect leads to a dampened amplitude of the seasonal cycle in the SH and an intensified

Atmospheric
Chemistry
and Physics
Discussions

537   in the NH. This can have an impact on the distribution of stratospheric ozone in the troposphere:

538   in the SH more ozone is transported into the troposphere in winter, when the chemical lifetimes

539   are relatively long, whereas in the NH the largest increase is found in summer. This may explain

540   the larger increase of O3s columns in the SH compared to the NH despite the smaller increase

541   in ozone mass flux (see Table 2 and 3).

542   The future spatial distribution of the tropospheric O3s column in the troposphere is determined

543   by the change pattern due to GHG increases. Here, the largest increase of O3s mixing ratios

544   occurs in the subtropical upper troposphere, where stratospheric ozone is transported into the

545   troposphere via tropopause folds and then further down to lower levels in the large-scale sinking

546   of the Hadley cell (Roelofs and Lelieveld, 1997). ODS-related changes in the tropospheric O3s

547   column are smaller. They show no comparable signal in the subtropical region, but a more

548   homogeneous distribution. In the ODS simulation, the main increase of stratospheric ozone

549   input occurs via the downward branch of the BDC in middle and higher latitudes, where the

550   chemical ozone loss of tropospheric ozone is smaller than in the subtropics and hence mixing

551   towards the surface is more efficient.

552   In the SH winter months, the ozone change due to increased stratospheric ozone influx explains

553   up to 80 % of the overall tropospheric ozone increase under the RCP8.5 scenario by the end of

554   the century. In the rest of the year, the stratospheric ozone changes cover more than 50 % of

555   the ozone changes in the SH troposphere. In contrast, increased stratospheric ozone explains

556   only about 70 % of the ozone changes in NH spring indicating the strong increase of

557   tropospheric photochemical ozone production in the future due to the doubling of methane

558   emissions under the RCP8.5 scenario.

559   The comparison with the transient EMAC simulation under the RCP6.0 scenario shows a

560   smaller future increase in annual global ozone mass flux into the troposphere (4.2 %/decade)

Atmospheric
Chemistry
and Physics
Discussions

561   than under the RCP8.5 scenario (5.3 %/decade). In the transient RCP6.0 simulation the positive

562   trend between 2000 and 2100 is larger in the SH than in the NH, which is not found in the

563   RCP8.5 timeslices. The stronger increase in the ozone mass flux under the RCP8.5 scenario is

564   connected with a larger O3s column, but the relative contribution of O3s to ozone in the

565   troposphere rises similarly in both scenarios. This is caused by the different evolution of the

566   ozone produced in the troposphere in the RCP6.0 and RCP8.5 scenario. In the past, the input of

567   stratospheric ozone has slightly decreased between 1960 and 1999, especially in the SH (-1.4

568   %/decade) due to the formation of the ozone hole. However, the O3s column in the troposphere

569   integrated over the NH and the SH shows a small positive trend. This may be related with the

570   seasonal timing of the changes, since ozone loss in the SH stratosphere has the largest effect on

571   the ozone mass flux in spring and early summer when the tropospheric ozone loss rates are

572   higher than in winter and mixing is less efficient anyway.

573   In summary, this study shows that GHG and ODS changes have different effects on the future

574   ozone mass flux, the seasonality and the resulting abundances of stratospheric ozone in the

575   troposphere. Moreover, it shows that both forcings are projected to cause an increased amount

576   of stratospheric ozone in the troposphere, which will not only contribute to the radiative forcing

577   and global warming but will also affect the air quality at the surface.

578

579   **Code availability**

580   The Modular Earth Submodel System (MESSy), including the EMAC model, is continuously

581   further developed and applied by a consortium of institutions. The usage of MESSy and access

582   to the source code is licensed to all affiliates of institutions, which are members of the MESSy

583   Consortium. Institutions can become a member of the MESSy Consortium by signing the

584   MESSy Memorandum of Understanding. More information can be found on the MESSy

585   Consortium website (http://www.messy-interface.org).

586

Data availability

588   The data of the ESCiMo simulation RC2-base-05 will be made available in the Climate and

589   Environmental Retrieval and Archive (CERA) database at the German Climate Computing

590   Centre (DKRZ; http://cera-www.dkrz.de/WDCC/ui/Index.jsp). The corresponding digital

591   object identifiers (doi) will be published on the MESSy Consortium web page

592   (http://www.messy-interface.org). A subset of the RC2-base-05 simulation results has been

593   uploaded to the BADC database for the CCMI project. Data of the EMAC timeslice simulations

594   performed for this for this paper are available at the Freie Universität Berlin on the SHARP

595   data archive under ACPD_ozone_transport_Meul_et_al_2018.tar.

596

Author contribution

598   SM has performed and analysed the timeslice simulations and has written the manuscript. UL

599   has initialized the study and has considerably contributed to the manuscript and the discussion.

600   PK has contributed to the analysis of the model data. SOH has performed the timeslice

601   simulations and has contributed to the discussion of the results. PJ led the ESCiMo project,

602   coordinated the preparation of the EMAC simulation setups and conducted the model

603   simulations (here RC2-base-05). Moreover, he contributed to the EMAC model development,

604   including the here applied O3s diagnostics.

605

Atmospheric
Chemistry
and Physics
Discussions

Open Access

EGU

Competing interests

607 The authors declare that they have no conflict of interest.

608

Special issue statement

610 This article is part of the special issue "The Modular Earth Submodel System (MESSy)

611 (ACP/GMD inter-journal SI)". It is not associated with a conference.

612

Acknowledgements

623

624

References

626 Akritidis, D., Pozzer, A., Zanis, P., Tyrlis, E., Škerlak, B., Sprenger, M., and Lelieveld, J.: On

627   the role of tropopause folds in summertime tropospheric ozone over the eastern

27

628   Mediterranean and the Middle East, Atmos. Chem. Phys., 16, 14025-14039,

629   doi:10.5194/acp-16-14025-2016, 2016.

630   Appenzeller, C., J. R. Holton, and K. H. Rosenlof: Seasonal variation of mass transport across

631   the tropopause, J. Geophys. Res., 101(D10), 15071-15078, doi:10.1029/96JD00821, 1996.

632   Banerjee, A., Maycock, A. C., Archibald, A. T., Abraham, N. L., Telford, P., Braesicke, P., and

633   Pyle, J. A.: Drivers of changes in stratospheric and tropospheric ozone between year 2000

634   and 2100, Atmos. Chem. Phys., 16, 2727-2746, doi:10.5194/acp-16-2727-2016, 2016.

635   Barré, J., El Amraoui, L., Ricaud, P., Lahoz, W. A., Attié, J.-L., Peuch, V.-H., Josse, B., and

636   Marécal, V.: Diagnosing the transition layer at extratropical latitudes using MLS O3 and

637   MOPITT CO analyses, Atmos. Chem. Phys., 13, 7225-7240, doi:10.5194/acp-13-7225-

638   2013, 2013.

639   Butchart, N., I. Cionni, V. Eyring, T. G. Shepherd, D. W. Waugh, H. Akiyoshi, J. Austin, C.

640   Brühl, M. P. Chipperfield, E. Cordero, M. Dameris, R. Deckert, S. Dhomse, S. M. Frith, R.

641   R. Garcia, A. Gettelman, M. A. Giorgetta, D. E. Kinnison, F. Li, E. Mancini, C. McLandress,

642   S. Pawson, G. Pitari, D. A. Plummer, E. Rozanov, F. Sassi, J.F. Scinocca, K. Shibata, B.

643   Steil, and W. Tian: Chemistry-Climate Model Simulations of Twenty-First Century

644   Stratospheric Climate and Circulation Changes, J. Clim., 23, 5349-5374, 2010.

645   Butchart. N. and Scaife. A.: Removal of chlorofluorocarbons by increased mass exchange

646   between the stratosphere and troposphere in a changing climate, Nature, 410, 799-801,

647   doi:10.1038/35071047, 2010.

648   Collins, W. J., R. G. Derwent, C. E. Johnson, and D. S. Stevenson: The impact of human

649   activities on the photochemical production and destruction of tropospheric ozone, Q. J. R.

650   Meteorol. Soc., 126, 1925-1951, 2000.

Atmospheric
Chemistry
and Physics
Discussions

Open Access

EGU

651 Collins, W. J., R. G. Derwent, B. Garnier, C. E. Johnson, M. G. Sanderson, and D. S. Stevenson:

652 Effect of stratosphere-troposphere exchange on the future tropospheric ozone trend, J.

653 Geophys. Res., 108(D12), 8528, doi:10.1029/2002JD002617, 2003.

654 Collins, W. J., Bellouin, N., Doutriaux-Boucher, M., Gedney, N., Halloran, P., Hinton, T.,

655 Hughes, J., Jones, C. D., Joshi, M., Liddicoat, S., Martin, G., O'Connor, F., Rae, J., Senior,

656 C., Sitch, S., Totterdell, I., Wiltshire, A., and Woodward, S.: Development and evaluation

657 of an Earth-System model – HadGEM2, Geosci. Model Dev., 4, 1051–1075,

658 doi:10.5194/gmd-4-1051-2011, 2011.

659 Fischer, H., Wienhold, F. G., Hoor, P., Bujok, O., Schiller, C., Siegmund, P., Ambaum, M.,

660 Scheeren, H. A. and Lelieveld, J.: Tracer correlations in the northern high latitude lowermost

661 stratosphere: Influence of cross-tropopause mass exchange, *Geophysical Research Letters*,

662 27, 1, 97-100, DOI = 10.1029/1999GL010879, 2000.

663 Giorgetta, M. A. and Bengtsson, L.: Potential role of the quasi-biennial oscillation in the

664 stratosphere-troposphere exchange as found in water vapor in general circulation model

665 experiments, J. Geophys. Res.-Atmos., 104, 6003–6019, doi:10.1029/1998JD200112, 1999.

666 Giorgetta, M. A., et al.: Climate and carbon cycle changes from 1850 to 2100 in MPI-ESM

667 simulations for the Coupled Model Intercomparison Project phase 5, J. Adv. Model. Earth

668 Syst., 5, 572–597, doi:10.1002/jame.20038, 2013.

669 Hegglin, M. I., and T. G. Shepherd: O3-N2O correlations from the Atmospheric Chemistry

670 Experiment: Revisiting a diagnostic of transport and chemistry in the stratosphere, J.

671 Geophys. Res., 112, D19301, doi:10.1029/2006JD008281, 2007.

672 Hegglin, M. and T. Shepherd: Large climate-induced changes in ultraviolet index and

673 stratosphere-to-troposphere ozone flux, Nature Geosci., 2, 687 – 691,

674 DOI:10.1038/ngeo604, 2009.

675   Holton, J. R., P. H. Haynes, M. E. McIntyre, A. R. Douglass, R. B. Rood, and L. Pfister:

676   Stratosphere-troposphere exchange, Rev. Geophys., 33(4), 403–439, 1995.

677   Intergovernmental Panel on Climate Change: Climate change 2001: The scientific basis,

678   Contribution of Working Group 1 to the Third Assessment Report, Cambridge, United

679   Kingdom and New York, NY, USA, 2001.

680   Jöckel, P., Tost, H., Pozzer, A., Brühl, C., Buchholz, J., Ganzeveld, L., Hoor, P., Kerkweg, A.,

681   Lawrence, M. G., Sander, R., Steil, B., Stiller, G., Tanarhte, M., Taraborrelli, D., van

682   Aardenne, J., & Lelieveld, J.: The atmospheric chemistry general circulation model

683   ECHAM5/MESSy1: consistent simulation of ozone from the surface to the mesosphere,

684   Atmospheric Chemistry and Physics, 6, 5067–5104, doi: 10.5194/acp-6-5067-2006, URL

685   http://www.atmos-chem-phys.net/6/5067/2006/, 2006.

686   Jöckel, P., Tost, H., Pozzer, A., Kunze, M., Kirner, O., Brenninkmeijer, C. A. M., Brinkop, S.,

687   Cai, D. S., Dyroff, C., Eckstein, J., Frank, F., Garny, H., Gottschaldt, K.-D., Graf, P., Grewe,

688   V., Kerkweg, A., Kern, B., Matthes, S., Mertens, M., Meul, S., Neumaier, M., Nützel, M.,

689   Oberländer-Hayn, S., Ruhnke, R., Runde, T., Sander, R., Scharffe, D., and Zahn, A.: Earth

690   System Chemistry integrated Modelling (ESCiMo) with the Modular Earth Submodel

691   System (MESSy) version 2.51, Geosci. Model Dev., 9, 1153-1200, doi:10.5194/gmd-9-

692   1153-2016, 2016.

693   Johnson, C. E., Collins, W. J., Stevenson, D. S., and Derwent, R. G.: Relative roles of climate

694   and emissions changes on future tropospheric oxidant concentrations, J. Geophys. Res.-

695   Atmos., 104, 18631–18645, doi:10.1029/1999JD900204, 1999.

696   Jonsson, A. I., J. de Grandpré, V. I. Fomichev, J. C. McConnell and S. R. Beagley: Doubled

697   CO2-induced cooling in the middle atmosphere: Photochemical analysis of the ozone

698   radiative feedback, J. Geophys. Res., 109, D24103, doi:10.1029/2004JD005093, 2004.

Atmospheric
Chemistry
and Physics
Discussions

Open Access

EGU

699   (The HadGEM2 Development Team): Martin, G. M., Bellouin, N., Collins, W. J., Culverwell,

700   I. D., Halloran, P. R., Hardiman, S. C., Hinton, T. J., Jones, C. D., McDonald, R. E.,

701   McLaren, A. J., O'Connor, F. M., Roberts, M. J., Rodriguez, J. M., Woodward, S., Best, M.

702   J., Brooks, M. E., Brown, A. R., Butchart, N., Dearden, C., Derbyshire, S. H., Dharssi, I.,

703   Doutriaux-Boucher, M., Edwards, J. M., Falloon, P. D., Gedney, N., Gray, L. J., Hewitt, H.

704   T., Hobson, M., Huddleston, M. R., Hughes, J., Ineson, S., Ingram, W. J., James, P. M.,

705   Johns, T. C., Johnson, C. E., Jones, A., Jones, C. P., Joshi, M. M., Keen, A. B., Liddicoat,

706   S., Lock, A. P., Maidens, A. V., Manners, J. C., Milton, S. F., Rae, J. G. L., Ridley, J. K.,

707   Sellar, A., Senior, C. A., Totterdell, I. J., Verhoef, A., Vidale, P. L., and Wiltshire, A.: The

708   HadGEM2 family of Met Office Unified Model climate configurations, Geosci. Model Dev.,

709   4, 723–757, doi:10.5194/gmd-4-723-2011, 2011.

710   Meinshausen, M., S. J. Smith, K. V. Calvin, J. S. Daniel, M. L. T. Kainuma, J.-F. Lamarque,

711   K. Matsumoto, S. A. Montzka, S. C. B. Raper, K. Riahi, A. M. Thomson, G. J. M. Velders

712   and D. van Vuuren: The RCP Greenhouse Gas Concentrations and their Extension from

713   1765 to 2300, Climatic Change (Special Issue), doi: 10.1007/s10584-011-0156-z, 2011.

714   Meul, S., M. Dameris, U. Langematz, J. Abalichin, A. Kerschbaumer, A. Kubin, and S.

715   Oberländer-Hayn: Impact of rising greenhouse gas concentrations on future tropical ozone

716   and UV exposure, Geophys. Res. Lett., 43, 2919–2927, doi:10.1002/2016GL067997, 2016.

717   Neu, J. L., T. Flury, G. L. Manney, M. L. Santee, N. J. Livesey, and J. Worden: Tropospheric

718   ozone variations governed by changes in stratospheric circulation, Nat. Geosci, 7(5), 340-

719   344, doi:10.1038/ngeo2138, 2014.

720   Oberländer, S., U. Langematz, and S. Meul: Unraveling impact factors for future changes in

721   the Brewer-Dobson circulation, J. Geophys. Res. Atmos., *118*, doi: 10.1002/jgrd.50775,

722   2013.

Atmospheric
Chemistry
and Physics
Discussions

Open Access

723 Olsen, M. A., A. R. Douglass, and M. R. Schoeberl: Estimating downward cross-tropopause

724   ozone flux using column ozone and potential vorticity, J. Geophys. Res., 107(D22), 4636,

725   doi:10.1029/2001JD002041, 2002.

726 Ordóñez, C., D. Brunner, J. Staehelin, P. Hadjinicolaou, J. A. Pyle, M. Jonas, H. Wernli, and

727   A. S. H. Prévôt: Strong influence of lowermost stratospheric ozone on lower tropospheric

728   background ozone changes over Europe, Geophys. Res. Lett., 34, L07805,

729   doi:10.1029/2006GL029113, 2007.

730 Roelofs, G.-J. and Lelieveld, J.: Model study of the influence of cross-tropopause O_3 transports

731   on tropospheric O_3 levels, Tellus B, 49, 38–55, 1997.

732 Sander, R., Baumgaertner, A., Gromov, S., Harder, H., Jöckel, P., Kerkweg, A., Kubistin, D.,

733   Regelin, E., Riede, H., Sandu, A., Taraborrelli, D., Tost, H., and Xie, Z.-Q.: The atmospheric

734   chemistry box model CAABA/MECCA-3.0, Geosci. Model Dev., 4, 373–380,

735   doi:10.5194/gmd-4-373-2011, 2011a.

736 Sander, S. P., Abbatt, J., Barker, J. R., Burkholder, J. B., Friedl, R. R., Golden, D. M., Huie, R.

737   E., Kolb, C. E., Kurylo, M. J., Moortgat, G. K., Orkin, V. L., and Wine, P. H.: Chemical

738   Kinetics and Photochemical Data for Use in Atmospheric Studies, Evaluation No. 17, JPL

739   Publication   10-6,   Jet   Propulsion   Laboratory,   Pasadena,   available   at:

740   http://jpldataeval.jpl.nasa.gov (last access: 23 March 2016), 2011b.

741 Shindell, D. T., et al.: Simulations of preindustrial, present-day, and 2100 conditions in the

742   NASA GISS composition and climate model G-PUCCINI, Atmos. Chem. Phys., 6, 4427–

743   4459, 2006.

744 Schmidt, H., S. Rast, F. Bunzel, M. Esch, M. Giorgetta, S. Kinne, T. Krismer, G. Stenchikov,

745   C. Timmreck, L. Tomassini, and M. Walz: Response of the middle atmosphere to

746   anthropogenic and natural forcings in the CMIP5 simulations with the Max Planck Institute

747   Earth system model, J. Adv. Model. Earth Syst., 5, 98–116, doi:10.1002/jame.20014, 2013.

748   Škerlak, B., Sprenger, M., and Wernli, H.: A global climatology of stratosphere-troposphere

749   exchange using the ERA-Interim data set from 1979 to 2011, Atmos. Chem. Phys., 14, 913-

750   937, doi:10.5194/acp-14-913-2014, 2014.

751   Stohl, A., et al.: Stratosphere-troposphere exchange: A review, and what we have learned from

752   STACCATO, J. Geophys. Res., 108 (D12), 8516, doi:10.1029/2002JD002490, 2003.

753   Sudo, K., M. Takahashi, and H. Akimoto: Future changes in stratosphere-troposphere exchange

754   and their impacts on future tropospheric ozone simulations, Geophys. Res. Lett., 30(24),

755   2256, doi:10.1029/2003GL018526, 2003.

756   Tian, W., M. P. Chipperfield, D. S. Stevenson, R. Damoah, S. Dhomse, A. Dudhia, H.

757   Pumphrey, and P. Bernath: Effects of stratosphere-troposphere chemistry coupling on

758   tropospheric ozone, J. Geophys. Res., 115, D00M04, doi:10.1029/2009JD013515, 2010.

759   WMO (World Meteorological Organisation): Scientific Assessment of Ozone Depletion: 2010,

760   Global Ozone Research and Monitoring Project-Report No. 52, 516 pp., World Meteorol.

761   Organ., Geneva, Switzerland, 2011.

762   WMO (World Meteorological Organisation): Scientific Assessment of Ozone Depletion: 2014,

763   Global Ozone Research and Monitoring Project-Report No. 55, 416 pp., World Meteorol.

764   Organ., Geneva, Switzerland, 2014.

765   Young, P. J., Archibald, A. T., Bowman, K. W., Lamarque, J.-F., Naik, V., Stevenson, D. S.,

766   Tilmes, S., Voulgarakis, A., Wild, O., Bergmann, D., Cameron-Smith, P., Cionni, I., Collins,

767   W. J., Dalsøren, S. B., Doherty, R. M., Eyring, V., Faluvegi, G., Horowitz, L. W., Josse, B.,

768   Lee, Y. H., MacKenzie, I. A., Nagashima, T., Plummer, D. A., Righi, M., Rumbold, S. T.,

769   Skeie, R. B., Shindell, D. T., Strode, S. A., Sudo, K., Szopa, S., and Zeng, G.: Pre-industrial

770   to end 21st century projections of tropospheric ozone from the Atmospheric Chemistry and

771   Climate Model Intercomparison Project (ACCMIP), Atmos. Chem. Phys., 13, 2063-2090,

772   doi:10.5194/acp-13-2063-2013, 2013.

773   Zeng, G., and J. A. Pyle: Changes in tropospheric ozone between 2000 and 2100 modeled in a

774   chemistry-climate model, Geophys. Res. Lett., 30(7), 1392, doi:10.1029/2002GL016708,

775   2003.

776   Zeng, G., O. Morgenstern, P. Braesicke, and J. A. Pyle: Impact of stratospheric ozone recovery

777   on tropospheric ozone and its budget, Geophys. Res. Lett., 37, L09805,

778   doi:10.1029/2010GL042812, 2010.

779   **Table 1**. EMAC CCM simulations used in this study.

Name	Run mode	GHG	Tropos. O3 precursor	ODS	SST/SIC
RCP6.0 (referred to as RC2-base-05 in Jöckel et al., 2016)	Transient (1960-2099, after 10 years spinup)	RCP6.0	RCP6.0	Observations and A1	HadGEM 1960-2099
REF2000	Timeslice (40 years, after 5 years spinup)	Observations for 2000	Observations for 2000	Observations for 2000	MPI-ESM 1995-2004
REF2100	Timeslice (40 years, after 5 years spinup)	RCP8.5 for 2100	RCP8.5 for 2100	A1 for 2100	MPI-ESM 2095-2104
GHG2100	Timeslice (40 years, after 5 years spinup)	RCP8.5 for 2100	Observations for 2000	Obs. for 2000	MPI-ESM 2095-2104
ODS2100	Timeslice (40 years, after 5 years spinup)	Observations for 2000	Observations for 2000	A1 for 2100	MPI-ESM 1995-2004

Atmospheric
Chemistry
and Physics
Discussions

780   **Table 2**. Overview of the annual ozone mass flux into the troposphere and the corresponding

781   standard deviations in the EMAC timeslice simulations. Gray numbers indicate the change

782   relative to the REF2000 simulation.

	O3 mass flux [Tg/yr]		
	global mean	NH	SH
REF2000	712±26	390±18	322±16
REF2100	1088±43 +53%	598±29 +53%	490±23 +52%
GHG2100	1041± 36 +46%	590±28 +51%	451±26 +40%
ODS2100	758±26 +7%	406±20 +4%	352±13 +9%

783

784

785 **Table 3**. Overview of the annual mean tropospheric O3 and O3s burden [Tg] with the

786 corresponding standard deviations in the EMAC timeslice simulations. Grey numbers indicate

787 the change relative to the REF2000 simulation.

788

	Tropospheric O3 column [Tg]			Tropospheric O3s column [Tg]		
	global mean	NH	SH	global mean	NH	SH
REF2000	**401±2**	**222±2**	**179±1**	**182 ±3**	**96 ±2**	**86 ±2**
REF2100	**527±3** +31%	**290±2** +31%	**237±2** +32%	**258 ±4** +42%	**134 ±2** +40%	**123 ±2** +43%
GHG2100	**513±3** +28%	**282± 2** +27%	**231±2** +29%	**246 ±3** +35%	**128 ±2** +33%	**118 ±2** +37%
ODS2100	**409±2** +2%	**225±2** +1%	**184±1** +3%	**189 ±2** +4%	**98 ±1** 2%	**91 ±1** +6%

789

790

791

792

793

794

795

796

797

798

799

800

801

802

803

804

805

806

807

808 **Figure 1**: Top: O_3-CO scatter plot for the months January to December in the latitude band

809 30°-60°N for the REF2000 simulation from the troposphere to the lower stratosphere. Color

810 coding indicates different height regions. Bottom: O_3-N_2O scatter plot for the months

811 September to November in the Northern Hemisphere for the REF2000 simulation for the

812 altitude region between 270 and 0.1 hPa. Color coding indicates different latitude bands.
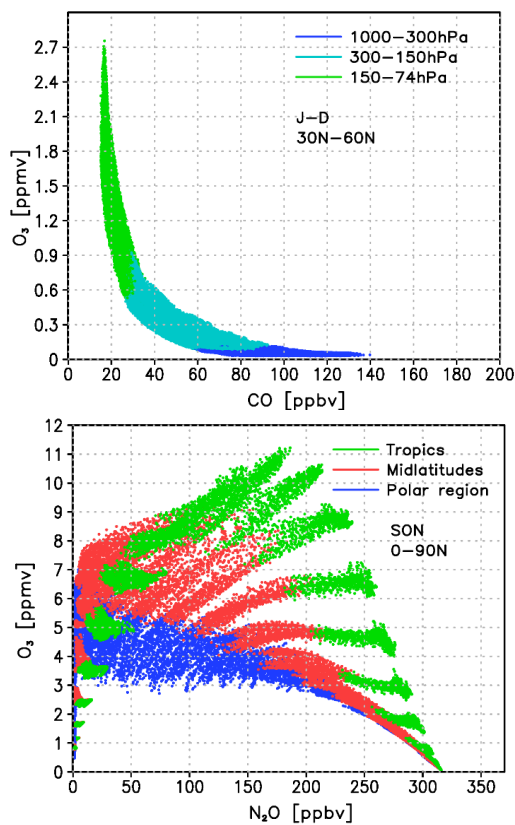
813

814

815

816

817

818

819

820

821

822

823

824

825

826

827

828

829

Figure 2: a) Annual ozone mass flux and its 95% confidence interval (i.e. $\pm 2\sigma$, with $\sigma :=$ standard deviation) [Tg/month] from the stratosphere into the troposphere (F_{out}) in the REF2000 simulation integrated globally (black), over the northern (red) and southern (blue) hemispheres. b) As a) but for F_{in} (the product between the ozone concentration and the negative zonal mean residual vertical velocity $\bar{w}^*$ at 91 hPa). c) As a) but for the negative monthly change in ozone mass of the LMS (-dM/dt), also referred to as seasonal breathing.

836

837

838

Atmospheric
Chemistry
and Physics
Discussions

839

840

853
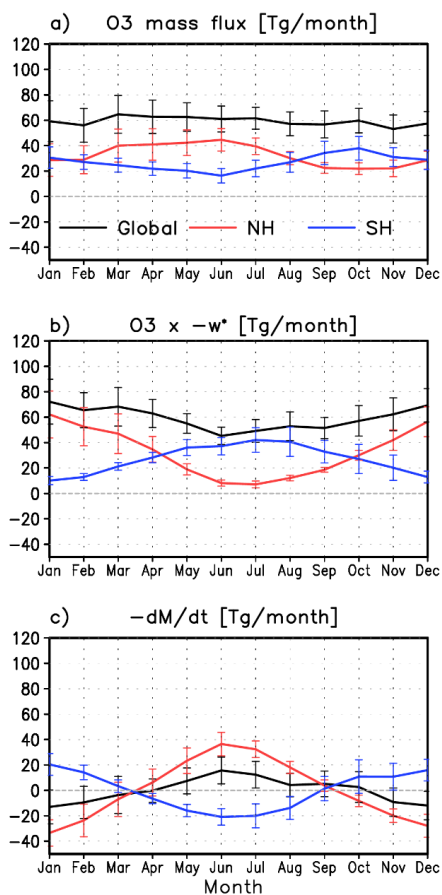
Figure 3: a) Geographical distribution of stratospheric partial columns of the diagnostic O3s tracer in Dobson Units (DU) in June for the REF2000 simulation. b) as a) but for the tropospheric columns. c) Latitude-height section of the O3s volume mixing ratios [ppbv] and d) latitude-height section of the chemical loss rate of O3s [ppbv/day]. The black dashed line indicates the position of the mean tropopause. Gray contour lines in c) show the relative contribution of O3s to the ozone field in %.

860

861

862

863

864
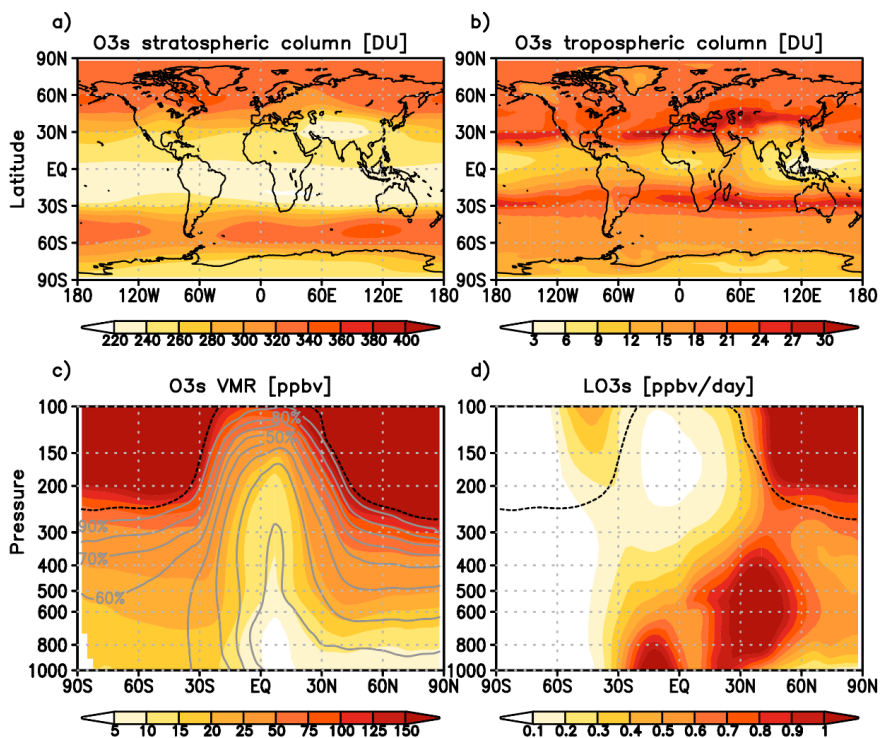
865

866

867

868

869

870

871

872

873

874
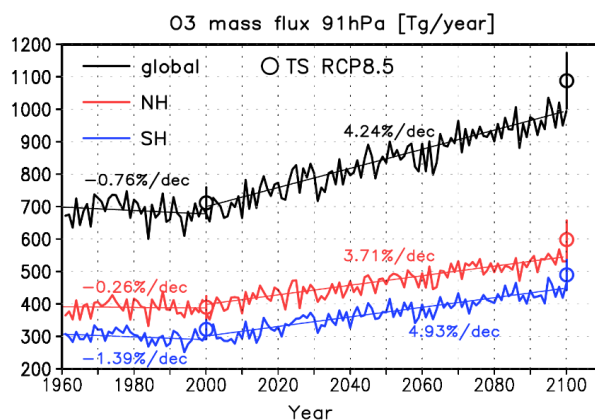
875   **Figure 4**: Temporal evolution of the ozone mass flux [Tg/year] from 1960 to 2099 in the

876   transient RCP6.0 simulation integrated globally (black), over the northern (red), and southern

877   (blue) hemispheres. The thin lines indicate the linear fits for the sub-periods 1960 to 2000 and

878   2000 to 2099. In addition, the ozone mass fluxes derived from the timeslice simulations (TS)

879   for the years 2000 (REF2000) and 2100 (REF2100, RCP8.5 scenario) are shown by open circles

880   including the $\pm\,2\sigma$ range.

881

Atmospheric
Chemistry
and Physics
Discussions

882

883

884

885

886

887

888

889

890

891

892

893

894

Figure 5: Annual cycle of ozone mass flux changes [Tg/month] in the timeslice simulations integrated globally (left), over the NH (middle), and over the SH (right) for the changes due to all forcings between 2000 and 2100 (top row), the effect of increasing GHG concentrations (middle row) and the impact of declining ODS levels (bottom row). The black error bars denote the $\pm 2\sigma$ standard deviation. The absolute ozone mass flux of the reference simulation REF2000 is shown as grey line with the corresponding y-axis on the right.

895

896

897

898
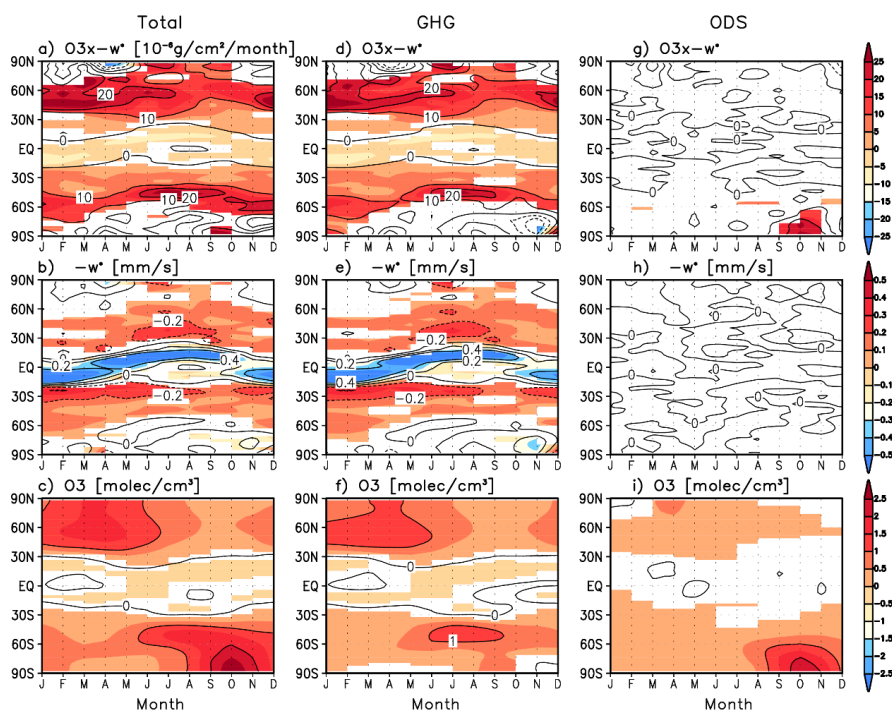
899

900

901

902

903

904

905

906

907
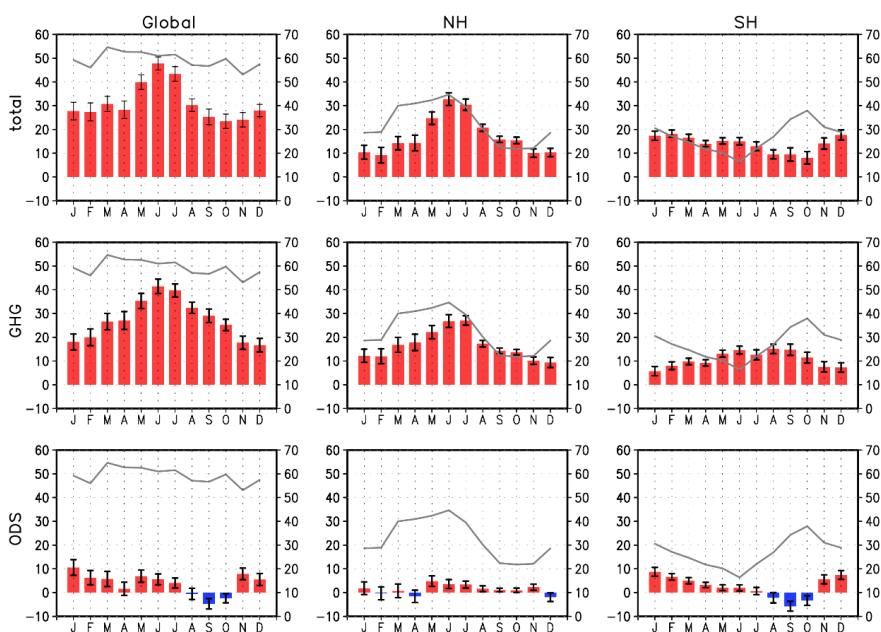
908

909

Figure 6: Annual cycle of the zonal mean change at 91 hPa in the timeslice simulations due to all forcings between 2000 and 2100 (left column), due to GHG increase (middle column), and due to ODS decrease (right column). Upper row: changes in the product of ozone concentration and $-\overline{w}^*$ [10^6 g/cm$^{2/}$month], which equals F_{in} when integrated over all latitudes. Middle row: changes in $-\overline{w}^*$ [mm/s]. Bottom row: changes in the ozone concentration [molecules/cm^2]. Significant changes on the 95 % confidence level are colored.

43

934
935
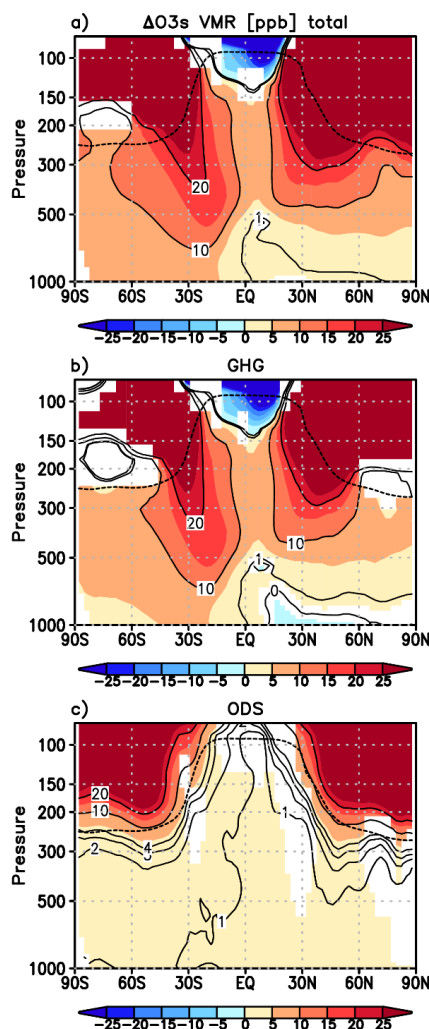936
937
938
939
940
941
942
943
944
945
946
947
948
949
950
951

952 **Figure 7**: Changes in the volume mixing ratios [ppbv] of the diagnostic tracer O3s for a) the

953 changes between 2000 and 2100 due to all forcings, b) the changes between 2000 and 2100 due

954 to increasing GHG concentrations and c) the changes between 2000 and 2100 due to declining

955 ODS levels for June (when the ozone mass flux is maximum in the NH and minimum in the

956 SH; see Fig. 2a). Significant changes on the 95 %-confidence level are colored. The black dotted

957 line represents the mean tropopause position in the REF2000 simulation. For the small ODS-

958 induced changes (c) additional contour lines (2, 3, and 4 ppbv) are shown.

959
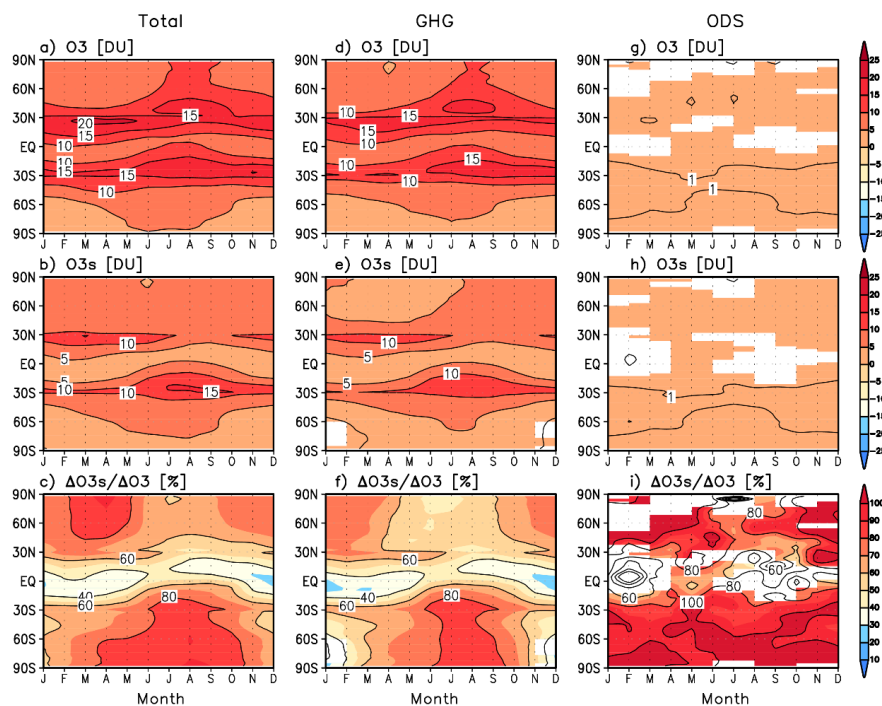
960

961

Figure 8: As Figure 6, but for the tropospheric ozone columns [DU] (upper row), the tropospheric columns of O3s [DU] (middle row), and the contribution of the O3s changes to the ozone changes between 2000 and 2100 [%] for the tropospheric column (bottom). Shading in the bottom row indicates the regions where both, O3s and ozone changes, are significant on the 95 % confidence level.

980

981

982

983

984

985

Atmospheric
Chemistry
and Physics
Discussions

986

987

988

989

990

991

992

993

994

995

996

997

998

999

1000

1001

1002

1003 **Figure 9**: a) Temporal evolution of the annual mean tropospheric column in ozone (solid) and

1004 O3s (dashed) [DU] averaged for the NH (red) and the SH (blue) in the transient RCP6.0

1005 simulation and the corresponding values of the reference timeslice simulations for the year 2000

1006 and 2100 (ozone: closed circle; O3s: open circle). b) Same as a) but for the ratio between O3s

1007 and O3 [%]. The black bars denote the $\pm 2\sigma$ range for the timeslice simulations. Note that the

1008 intra-annual variability in ozone and O3s is small in the timeslice simulations and the error bars

1009 are very short.

1010